crystals

MDPI

Communication

# Selective and Recyclable Sensing of Aqueous Phase 2,4,6-Trinitrophenol (TNP) Based on Cd(II) Coordination Polymer with Zwitterionic Ligand

**Kaimin Wang [1], Huaijun Tang [1,*], Donghua Zhang [1], Yulu Ma [2,*] and Yuna Wang [3]**

1 Key Laboratory of Comprehensive Utilization of Mineral Resources in Ethnic Regions, Key Laboratory of Green-Chemistry Materials in University of Yunnan Province, School of Chemistry & Environment, Yunnan Minzu University, Kunming 650500, Yunnan, China; kmwang041684@163.com (K.W.); ynmzdxzdh@163.com (D.Z.)

2 School of Pharmaceutical Sciences and Yunnan Key Laboratory of Pharmacology for Natural Products, Kunming Medical University, Kunming 650500, Yunnan, China; yuluma163@163.com

3 School of Chemical Science and Technology, Yunnan University, Kunming 650091, Yunnan, China; yndxwyn@163.com

* Correspondence: tanghuaijun@sohu.com (H.T.); yuluma163@163.com (Y.M.); Tel.: +86-871-6591-3043 (H.T.)

Received: 8 October 2018; Accepted: 27 November 2018; Published: 7 December 2018

**Abstract:** A novel coordination polymer, {[$Cd_4$(Dccbp)$_4$]·$H_2O$} (**1**) (Dccbp = 3,5-dicarboxy-1-(3-carboxybenzyl)pyridin-1-ium) was synthesized under hydrothermal conditions by a zwitterionic organic ligand and characterized by single crystal X-ray diffraction, infrared spectrum (IR), thermogravimetric analysis (TG), powder X-ray diffraction (PXRD) and luminescence. Complex **1** with a pyridine cation basic skeleton has the potential to serve as the first case of a luminescent material based on the zwitterionic type of organic ligand for selective, sensitive, and recyclable sensing of 2,4,6-trinitrophenol in the aqueous phase.

**Keywords:** coordination polymer; 2,4,6-trinitrophenol; sensor; luminescence; zwitterionic ligand

## 1. Introduction

Since the end of the 20th century, considerable attention has been paid to synthesis and characterization of novel coordination polymers (CPs) as well as metal-organic framework (MOFs) with fascinating structures and diverse functions [1–8]. An important feature is that the choice of appropriate ligands plays a very crucial role in the construction of CPs with specific structures, which promoted chemists to design new ligands and study their coordination chemistry [9]. Recently, the zwitterionic type of organic ligands, which possess dispersed positive charges and negative charges synchronously on the organic basic framework, have drawn chemists attention to construct functional CPs with various potential applications such as in gas separation [10], chemical catalysis [11], chemical separations [12], magnetism [13], optical properties [14,15], biological application [16], and so on [17–20]. Compared with the conventional neutral ligands, the zwitterionic types of organic ligands have obvious advantages owing to their good solubility, improved adsorption selectivity of guest molecules, and strong coordination ability. However, to date, only limited CPs based on zwitterionic organic ligands have been demonstrated. Therefore, the CPs based on this class of ligands still need further exploration.

2,4,6-Trinitrophenol (TNP) is a high explosive substance known to all which has been extensively used in commercial production processes such as dye, leather, and medicines industries [21,22]. However, due to its strong explosive capacity, TNP could also be used for fireworks and terrorist attacks [23]. Apart from its explosive nature, the presence of TNP above the legal limits causes skin/eye irritation, headaches, anaemia and liver injury [24]. Therefore, the development of new materials for

detection of TNP is critical in terms of anti-terrorist and environment considerations. Although various sophisticated methods [25] such as gas phase chromatography, elemental analysis, plasma laser sensor and ion mobility spectrometer have been developed for explosives detection, these advanced analysis and testing techniques are limited by their inconvenient to carry, time-consuming and tedious operation, high cost and not real-time monitoring drawbacks [26]. Compared with the traditional detection methods, the fluorescence detection based on coordination complexes has the advantages of high sensibility, easy synthesis, low cost and simple operation [27]. In the past few years, a large number of fluorescent probes for the detection of TNP explosive based on coordination polymers have been invented [28–30], most of which were operated in gaseous phase or in organic solvents, whereas water phase detection is rarely studied [31,32]. Aqueous phase recognition is rarely reported, mainly due to the poor stability of most CPs in the aqueous phase and fluorescence quenching in the aqueous phase. Taking account of the above reasons, it is still a major challenge to synthesize CP-based fluorescent probes for highly selective recognition of TNP in aqueous phase [33].

With these considerations in mind, we selected the zwitterionic type of organic ligand 3,5-dicarboxy-1-(3-carboxybenzyl)pyridin-1-ium chloride ($H_3DccbpCl$) to construct a new Cd(II) coordination polymer {$[Cd_4(Dccbp)_4]\cdot H_2O$}. As far as we know, this luminescent probe has the potential as a first case of a zwitterionic organic ligand-based luminescent CP material for the selective, sensitive and recyclable detection of TNP in water.

## 2. Experimental Section

### *2.1. Material and Methods*

All of the reagents and solvents used in this paper were purchased from Adamas-beta Corporation Limited (Shanghai, China) and used as received without further purification, unless otherwise indicated. Crystallographic data were collected at 296 K on a Bruker Smart AXS CCD (Munich, Germany) diffractometer with graphite-monochromated Mo K$\alpha$ radiation ($\lambda$ = 0.71073 Å) using $\omega$-scan technique. Cell parameters were retrieved using SMART software and refined with SAINT on all observed reflections. Absorption corrections were applied with the program SADABS. The NMR spectra were recorded on a Bruker DRX400 (Billerica, MA, USA) ($^1$H: 400 $MH_Z$, $^{13}$C: 100 $MH_Z$), chemical shifts ($\delta$) are expressed in ppm, and deuterated DMSO was used as solvent. IR spectra were recorded on a FT-IR Thermo Nicolet Avatar 360 (Waltham, MA, USA) using KBr pellet. Elemental analyses of C, H, and N were determined on an Elementar Vario III EL elemental analyzer (Elementar, Langenselbold, Germany). The phase purity of the samples was investigated by powder X-ray diffraction (PXRD) measurements carried out on a Bruker D8-Advance diffractometer (Munich, Germany) equipped with CuK$\alpha$ radiation ($\lambda$ = 1.5406 Å) at a scan speed of 1°/min. Thermal stability studies were carried out on a NETSCHZ STA-449C (Bavaria, Germany) thermoanalyzer with a heating rate of 10°C/min under a nitrogen atmosphere. All luminescent analyses were performed on a F-7000 (Hitachi, Tokyo, Japan) fluorescent spectrometer.

### *2.2. Synthetic Procedures*

#### 2.2.1. Synthesis of 3,5-dicarboxy-1-(3-carboxybenzyl)pyridin-1-ium chloride ($H_3DccbpCl$)

A mixture of 3,5-pyridinedicarboxylic acid (1.671 g, 10.0 mmol) and 3-(chloromethyl)benzoic acid (1.877 g, 11.0 mmol) in *N*,*N*′-dimethylformamide (DMF) (50 mL) was refluxed for 24 h. When the reaction system was cooled to room temperature, a large amount of white precipitate was formed. Then filter and use *N*,*N*′-dimethylformamide (20 mL × 3) first, then wash the white precipitate with acetone (20 mL) and then dry naturally to afford $H_3DccbpCl$ (3.102 g, 92%). $^1$H NMR (400 Hz, DMSO-*d*6 + DCl): $\delta$= 9.91 (s, 2H, ArH), 9.15 (s, 1H, ArH), 8.30 (s, 1H, ArH), 8.03 (d, 1H, ArH), 7.96 (d, 1H, ArH), 7.66 (t, 1H, ArH), 6.24 (s, 2H, $CH_2$); $^{13}$C NMR (100 Hz, DMSO-*d*6 + DCl): $\delta$ = 167.1, 162.5,

148.8, 145.4, 134.3, 132.0, 132.0, 131.8, 130.8, 130.7, 130.1, 63.5. (Figure S1). Main IR (KBr, $cm^{-1}$): 3058, 1720, 1451, 1198, 902, 758, 700.

#### 2.2.2. Synthesis of {[$Cd_4$(Dccbp)$_4$]·$H_2O$} (**1**)

A solid mixture of $CdCl_2$ (55.0 mg), $H_3$DccbpCl (33.7 mg) and NaOH (12 mg) in 10 mL DMF/$H_2O$ solution ($v/v$ = 1:1) was encapsulated into 15 ml Teflon lined stainless steel autoclave. The reaction system was heated at 48h at 160 °C and cooled to room temperature at 5 °C/h. Colourless bulk crystals of the product were collected by filtration and washed several times with DMF/$H_2O$ solution ($v/v$ = 1:1) for drying in air. The obtained yield based on the $H_3$DccbpCl was 32.0%. Anal. Calcd for $C_{60}H_{38}Cd_4N_4O_{25}$ (1664.5735): C, 43.29; H, 2.30; N, 3.37. Found: C, 43.03; H, 2.39; N, 3.35. Main IR (KBr, $cm^{-1}$): 3377, 3052, 1667, 1551, 1382, 928, 760. (Figure S2)

### *2.3. Crystallography*

Using SHELXL-2014 direct method to solve structure **1**, we use SHELXL-2014 full matrix least square method to optimize F2 [34,35]. All non-hydrogen atoms are located in different Fourier synthesis and finally refined by anisotropic displacement parameters. The hydrogen atoms connected to the organic part are either self heterodyne Fourier map or fixed stereochemistry. The details of crystallographic data collection and refinement parameters are summarized in Table 1. Main bond lengths and angles are presented in Table 2. CCDC 1861292 (**1**) (Appendix A) contains the crystallographic data for this paper.

**Table 1.** Crystal data and structure refinement for **1**.

| Compound | **1** |
|---|---|
| Formula | C60H38Cd4N4O25 |
| Formula weight | 1664.54 |
| Crystal system | Monoclinic |
| $a$ | 7.8412(6) Å |
| $b$ | 11.2417(9) Å |
| $c$ | 15.6909(13) Å |
| $\alpha$ | 90° |
| $\beta$ | 94.8050(10)° |
| $\gamma$ | 90° |
| Unit cell volume | 1378.27(19) $Å^3$ |
| Space group | $P2_1/c$ |
| $Z$ | 1 |
| $D_X$/Mg $m^{-3}$ | 2.005 |
| $\mu$/$mm^{-1}$ | 1.620 |
| Reflections collected | 7278 |
| Independent reflections | 2909 |
| F(000) | 818 |
| $R_{int}$ | 0.0227 |
| GOF on $F^2$ | 1.166 |
| $R_1$, $wR_2$ [$I > 2\sigma(I)$] | 0.0257, 0.0516 |
| $R_1$, $wR_2$ [all data] | 0.0340, 0.0728 |
| CCDC number | 1861292 |

**Table 2.** Elected bond lengths (Å) and angles (°) for compound **1**.

| Bond lengths (Å) for **1** | | | |
|---|---|---|---|
| O(1)-Cd(1)C | 2.266(3) | O(4)-C(14) | 1.231(5) |
| Cd(1)-O(6) | 2.249(3) | O(4)-Cd(1)G | 2.253(3) |
| Cd(1)-O(4)A | 2.253(3) | O(5)-C(15) | 1.243(5) |
| Cd(1)-O(3)B | 2.254(3) | O(6)-C(15) | 1.256(5) |
| Cd(1)-O(1)C | 2.266(3) | N(1)-C(4) | 1.341(5) |

**Table 2.** *Cont.*

| Bond lengths (Å) for **1** | | | |
|---|---|---|---|
| Cd(1)-O(2)D | 2.274(3) | N(1)-C(3) | 1.347(5) |
| Cd(1)-O(5) | 2.554(4) | N(1)-C(6) | 1.478(5) |
| O(2)-Cd(1)E | 2.274(3) | C(1)-C(5) | 1.382(5) |
| O(3)-C(14) | 1.249(5) | C(1)-C(2) | 1.387(5) |
| O(3)-Cd(1)F | 2.254(3) | C(4)-C(5) | 1.382(5) |
| Bond angles (°) for **1** | | | |
| O(6)-Cd(1)-O(4)A | 82.77(12) | O(6)-Cd(1)-O(5) | 53.43(11) |
| O(6)-Cd(1)-O(3)B | 131.5(12) | O(4)A-Cd(1)-O(5) | 134.6(12) |
| C(4)-N(1)-C(3) | 121.0(3) | C(4)-N(1)-C(6) | 119.8(3) |
| O(4)A-Cd(1)-O(3)B | 145.6(13) | O(3)B-Cd(1)-O(5) | 78.67(11) |
| O(6)-Cd(1)-O(1)C | 100.7(13) | O(1)C-Cd(1)-O(5) | 112.8(13) |
| O(4)A-Cd(1)-O(1)C | 83.53(14) | O(2)D-Cd(1)-O(5) | 97.73(12) |
| O(3)B-Cd(1)-O(1)C | 90.48(13) | C(13)-O(1)-Cd(1)C | 136.1(3) |
| O(6)-Cd(1)-O(2)D | 108.9 (13) | C(13)-O(2)-Cd(1)E | 128.0(3) |
| O(4)A-Cd(1)-O(2)D | 84.76(14) | C(14)-O(3)-Cd(1)F | 140.6(3) |
| O(3)B-Cd(1)-O(2)D | 81.76(13) | C(14)-O(4)-Cd(1)G | 123.4(3) |
| O(1)C-Cd(1)-O(2)D | 146.4(12) | C(15)-O(5)-Cd(1) | 85.5(3) |
| C(3)-N(1)-C(6) | 119.1(3) | O(2)-C(13)-C(2) | 116.6(4) |
| C(5)-C(1)-C(2) | 120.0(4) | O(4)-C(14)-O(3) | 128.9(4) |
| O(1)-C(13)-O(2) | 128.0(4) | O(4)-C(14)-C(5) | 116.3(4) |
| O(1)-C(13)-C(2) | 115.4(4) | O(3)-C(14)-C(5) | 114.8(4) |

Symmetry transformations used to generate equivalent atoms for compound **1**: (A) x,−y+1/2,z+1/2; (B) −x+2,y−1/2, −z+1/2; (C) −x+2,−y+1,−z+1; (D) x,y−1,z; (E) x,y+1,z; (F) −x+2,y+1/2,−z+1/2; (G) x,−y+1/2,z−1/2.

## 3. Results

### *3.1. Crystal Structures*

#### 3.1.1. Descriptions of the Crystal Structures of {[$Cd_4$(Dccbp)$_4$]·$H_2O$} (1)

Coordination polymer **1** crystallizes in the $P2_1/c$ space group of the monoclinic system. Single-crystal X-ray diffraction analysis shows that **1** has a 2D (3, 6)-connected binodal layer. The asymmetric unit of **1** consists of one Cd(II) ion, one fully deprotonated Dccbp$^{2-}$ ligand and one lattice water molecule. Each Cd(II) ion adopts an interesting distorted triangular prism coordination geometry (Figure 1) and is coordinated by six carboxyl oxygen atoms (O5, O6, O1A, O3B, O2C and O4D) from five Dccbp$^{2-}$ ligands, with bond distances ranging from 2.249(3)–2.554(4) Å, and angles ranging from 82.77(12)–146.37(12)° (Figure 1). As shown in Figure S3, the three carboxylate groups of Dccbp$^{2-}$ ligand adopt two kinds of coordination modes, one of which is benzyl-COO group adopts chelating bidentate coordination mode, and the other two pyridyl-COO groups show bidentate bridging coordination fashion. In this compound, the Dccbp$^{2-}$ ligand exists in V-shaped conformation, with the dihedral angle of the benzene ring and the pyridine ring is about 85.02°, but the two aromatic rings are twisted with a torsion angle of C(4)-N(1)-C(6)-C(7) is 86.5°.

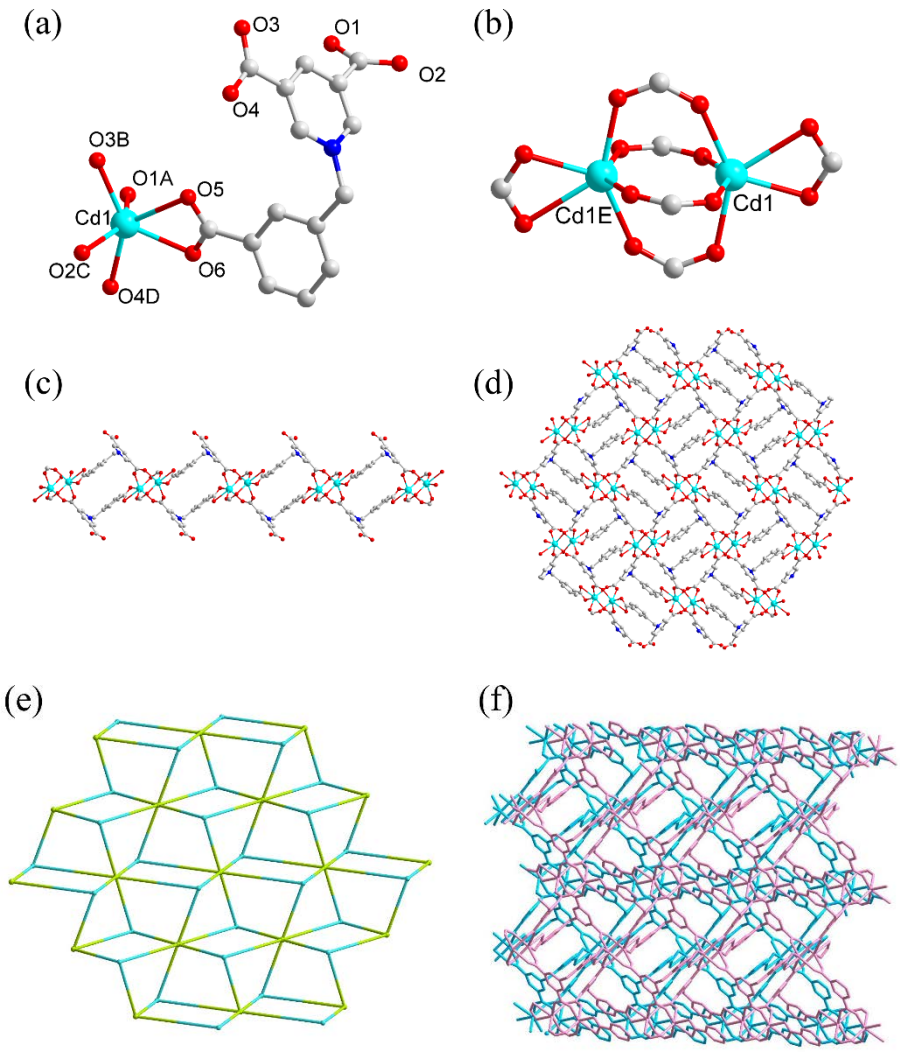


**Figure 1.** (**a**) Coordination environment of the {[$Cd_4$(Dccbp)$_4$]·$H_2O$} (coordination polymers (CP) **1**) (symmetry codes: (A) −x+2,−y+1,−z+1; (B) −x+2,y−1/2,−z+1/2; (C) x,y−1,z; (D) x,−y+1/2,z+1/2). (**b**) Coordination geometries of the dinuclear subunits generated by Cd1 atoms and carboxylate groups. (**c**) The One-dimensional infinite bead chain in CP **1**. (**d**) The 2-dimensional structure of CP **1**. (**e**) The kgd topology of **1**. (**f**)The 3D supramolecular architecture of **1**.

In this structure, two adjacent Cd(II) ions are joined by sharing four carboxylate groups of four Dccbp$^{2-}$ ligands in bidentate bridging coordination mode to form paddle-wheel-like dimers {$Cd_2$($\mu_2$-$CO_2$)$_4$}, with the Cd1···Cd1E distance of 3.5313(5) Å in it. The neighboring dinuclear subunits are connected by sharing two *trans* bridging Dccbp$^{2-}$ ligands to generate beaded chains along the *b* axis (Figure 1), which are further extended by pyridyl-COO and pyridine ring spacers in Dccbp$^{2-}$ ligands to produce a 2D (3, 6)-connected binodal net and its topological analysis suggests the presence of the overall structure has **kgd** topology. The 3D supramolecular architecture of compound **1** is obtained from the interlayer π···π stacking interactions between neighboring phenyl rings and benzene rings (centroid−centroid: 4.183 Å) (Figure S4).

### 3.1.2. Powder X-ray Power Diffraction (PXRD) and Thermogravimetric Analysis (TGA)

In order to determine whether the crystal structure truly represents the crystalline material tested in the performance study, Compound **1** was subjected to PXRD experiment at room temperature. As shown in Figure 2, the as-simulated patterns from the single-crystal data is consistent with the PXRD experimental ones in key positions, indicating that the good purity of the bulk crystal products

of **1**. To study the stabilities of CP **1**, thermogravimetric (TGA) analysis of **1** was developed under nitrogen atmosphere from room temperature to 800 °C (Figure S5). From 60 to 232 °C, the weight loss is 1.12% (calc. 1.08%) due to the loss of a molecule of free water. The frame structure of CP **1** began to decompose until about 370 °C, showing good thermal stability.

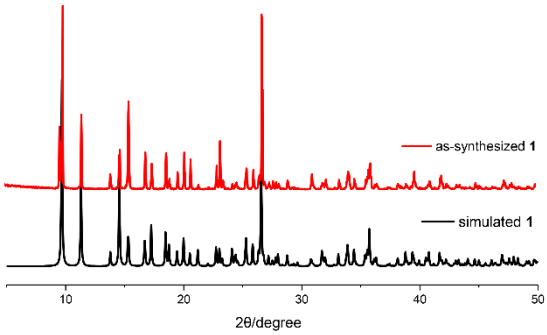


**Figure 2.** The powder X-ray diffraction (PXRD) patterns of **1**.

### *3.2. Solid-State Luminescence of Compound 1*

Considering CPs composed of $d^{10}$ metal centers with π-conjugated ligands are expected to have excellent luminescent properties, the solid state luminescent properties of the free $H_3$DccbpCl ligand and Compound 1 were recorded at ambient temperature. As shown in Figure 3, the free $H_3$DccbpCl ligand presents a broad emission band centered at 413 nm when excited at 356 nm, which is assigned to the typical π*–π transition of ligands. The fluorescence of complex **1** is similar to that of a free ligand, and when excited at 321 nm, an emission peak is shown at 407 nm. Compared to ligand emission, blue shift may be due to conformational changes of ligands when bound to metal ions [36,37].

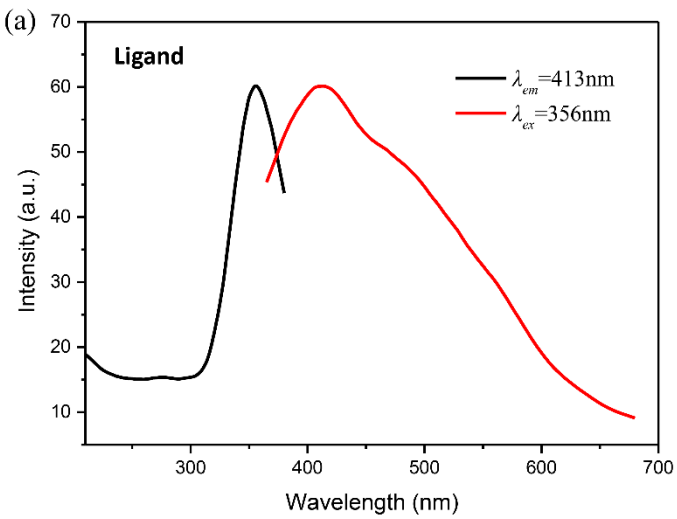


**Figure 3.** *Cont.*

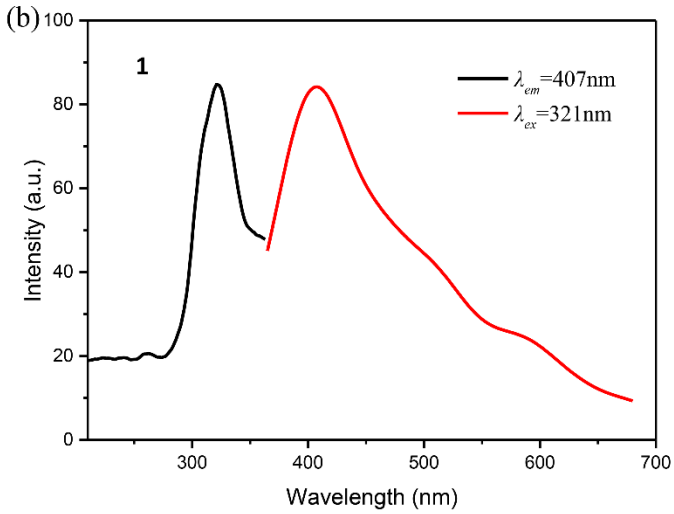


**Figure 3.** The solid state luminescent properties of (**a**) the free $H_3$DccbpCl ligand, (**b**) CP **1**.

### *3.3. Selective sensing of 2,4,6-Trinitrophenol*

The high luminescence intensity of the CP **1** prompts us to further investigate the potential luminescence sensing capability of **1** for TNP in aqueous phase. Firstly, the finely ground sample of **1** (10 mg) is immersed in the same concentration of different nitro compound being 50 μM (5 mL), then treated by sonication for 60 minutes followed by aging for 24 hours produced a stable suspension prior to the fluorescence study. The nitro compounds used are 2,4,6-trinitrophenol (TNP), 2,4-dinitrophenol (2,4-DNP), 4-nitrophenol (4-NP), 1,3-dinitrobenzene (*m*-DNB), 1,4-dinitrobenzene (*p*-DNB), 2,4-dinitrotoluene (2,4-DNT), 2,6-dinitrotoluene (2,6-DNT) and nitrobenzene (NM). All eight nitro analytes can weaken the luminescent intensity of **1** to a varying degree. Interestingly, a significant luminescence attenuation with a quench percentage (QP) of 86% is observed in the presence of TNP All nitro analytes tested in the experiment were able to attenuate the luminescence intensity of 1 to varying degrees. Interestingly, a significant luminescence decay of 86% QP (quench percentage) was observed in the presence of TNP (Figure 4a). However, the QP of 1 of 2,4-DNP, 4-NP, *m*-DNB, *p*-DNB, 2,4-DNT, 2,6-DNT and NM is 44%, 36%, 25%, 20%, 16%, 15%, 12%, respectively. These results clearly indicate that the sensitivity of **1** towards TNP is higher than that of other nitro analytes in aquatic systems.

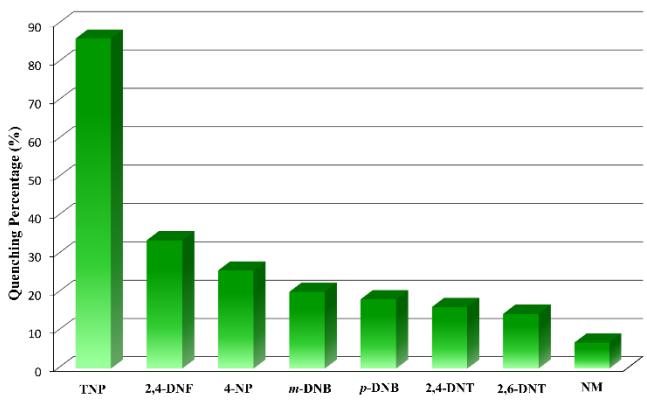


(**a**)

**Figure 4.** *Cont.*

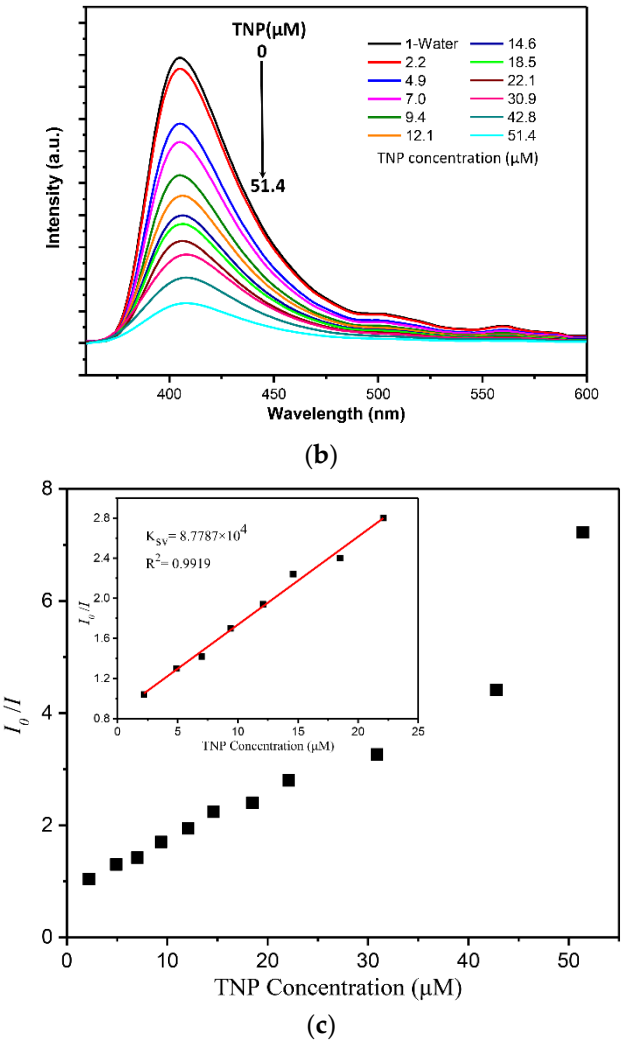


**Figure 4.** (**a**) Comparisons of the luminescence intensity of **1** in 50 μM different nitro analytes suspension in aqueous phase. (**b**) The luminescence spectra dispersed in water were titrated at room temperature by adding different concentrations of 2,4,6-trinitrophenol (TNP) (μM). (**c**) Relationship between Stern-Volmer plot of $I_o/I$ and TNP concentration in 1-water suspension.

In order to better understand the sensing ability of **1** for TNP, fluorescence quenching titration was further performed by recording the emission spectrum of the 1-aqueous suspension gradually added with TNP. As shown in Figure 4b, the intensity of luminescence at 407 nm decreased significantly as the concentration of TNP increased. In addition, the Stern-Volmer (SV) equation can be used to rationalize the low-concentration quenching effect: $I_o/I = 1 + Ksv \times [M]$, where $I_o$ and $I$ are the luminescence intensities in the absence and in the presence of the TNP, respectively; *K*sv is the quenching constant, and [M] is the molar concentration of TNP [38,39]. Interestingly, the SV plots were nearly linear at low concentration ($R^2$ = 0.9919), but a slight non-linear feature was produced at a higher concentration (Figure 4c, inset). The nonlinear characteristics in SV diagrams indicate the consolidation of the phenomena of dynamic and static quenching and/or energy transfer between **1** and TNP. This static quenching may be due to the electrostatic interactions between the pyridine cations of zwitterionic ligands and hydroxyl groups of TNP (Figure S6), while the dynamic one may be due to the collisional encounters between the fluorene moieties and TNP [40,41]. The possible reason for the luminescence quenching may be due to the photoinduced electron-transfer (PET) mechanism. The nitro compounds with electron-deficient property can obtain an electron from excited ligand (Figure S6), which is similar to that reported in previous work [42,43]. The *K*sv of **1** for TNP was calculated to be 8.7787 × $10^4$ $M^{-1}$ at

low concentrations, which is comparable to the highest values known for previously reported CP-based sensors, such as $[NH_2(CH_3)_2]_4[Zn_3(HBDPO)_2(SO_4)_2]$ ($1.2 \times 10^4$ $M^{-1}$) [44], $[Mg_3(1,4\text{-NDC})_4(u\text{-}H_2O)_2]$ ($1.5 \times 10^4$ $M^{-1}$) [45], $[Zn_4O\text{-}(bpt)_2(bdc)_{0.5}]$ ($1.69 \times 10^4$ $M^{-1}$) [46], and which clearly demonstrates the potential of **1** as a high sensitivity luminescent probe for TNP.

Additionally, taking into account the repeatability of chemical sensors is a very important parameter for practicality, the reproducibility of fluorescence detection on **1** was also investigated to find that **1** can be regenerated and reused at least five times after being sensed by centrifuging the dispersed crystals in water and washing several times in water (Figure 5). By monitoring the emission spectra of **1** disperse in the presence of 50 μM TNP, it is found that the quenching efficiency of each cycle is basically unchanged. Furthermore, the PXRD patterns of the **1** sample recovered after 5 cycles of detection showed the same patterns as the initial sample, indicating high stability of the material. (Figure S7). The above results indicate that **1** can be used as a fluorescent probe for TNP with high selectivity, sensitivity and recyclability.

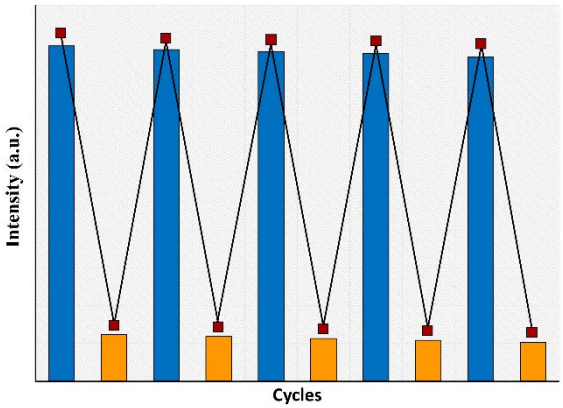


**Figure 5.** The quenching cycle test of **1** after adding 50 μM TNP in water.

## 4. Conclusions

In summary, a new type of luminescence probe based on coordination polymer **1** was successfully designed and synthesized under hydrothermal conditions by $d^{10}$ metal ($Cd^{2+}$) and a zwitterionic organic ligand. This material was used as a chemical sensor to detect various nitro analytes to find that CP **1** can provide an excellent fluorescent sensor for the highly selective and sensitive detection of TNP in water. Furthermore, since CP **1** can be easily regenerated by simply washing with water at least five cycles without gradually shrinking diminishing the fluorescence intensities and destroying the basic frame structure, it exhibits good recyclability. Although various luminescent CP materials detecting TNP in the vapour phase and/or organic solvents have already been reported, aqueous phase detection is rarely investigated. Considering the presence of TNP in the aqueous environment, the detection of TNP in an aquatic system designed in this article is more suitable for practical applications. Further research is being carried out in our laboratory.

**Supplementary Materials:** The following are available online at http://www.mdpi.com/2073-4352/8/12/456/s1, Figure S1: NMR spectrum of $H_3$DccbpCl Ligand. Figure S2: The infrared spectrum of $H_3$DccbpCl and CP **1**. Figure S3. Coordination modes of ligand in the coordination polymer **1**. Figure S4. The interlayer π···π stacking interactions in CP **1**. Figure S5: The thermogravimetric analysis of CP **1**. Figure S6. A possible schematic representation of the selective sensing and the simulation result of the electrostatic interaction between TNP and the monomer unit of coordination polymer **1**. Figure S7: Powder X-ray power diffraction patterns of CP **1** after five cycles detection of 2,4,6-Trinitrophenol.

**Author Contributions:** K.W. and H.T. are responsible for designing experiments and writing articles, Y.M. is responsible for doing synthesis experiments and analyzing the results, D.Z. and Y.W. are responsible for doing the other experiments. The above authors participated in the discussion process and approved the final manuscript.

**Funding:** This work was supported by the Yunnan Provincial Department of Education funded projects (2017ZZX085), the National Natural Science Foundation of China (Projects 21762049 and 21371151).

**Conflicts of Interest:** The authors declare no conflict of interest.

## Appendix A

CCDC 1861292 (**1**) contains the crystallographic data for this paper, which can be found from http://www.ccdc.cam.ac.uk/data_request/cif, or by e-mailing data_request@ccdc.cam.ac.uk.

## References


1. Liao, P.-Q.; Huang, N.-Y.; Zhang, W.-X.; Zhang, J.-P.; Chen, X.-M. Controlling guest conformation for efficient purification of butadiene. *Science* **2017**, *356*, 1193–1196. [CrossRef]
2. Serre, C.; Mellot-Draznieks, C.; Surble, S.; Audebrand, N.; Filinchuk, Y.; Ferey, G. Role of solvent-host interactions that lead to very large swelling of hybrid frameworks. *Science* **2007**, *315*, 1828–1831. [CrossRef]
3. Li, F.-L.; Shao, Q.; Huang, X.-Q.; Lang, J.-P. Nanoscale trimetallic metal-organic frameworks enable efficient oxygen evolution electrocatalysis. *Angew. Chem. Int. Ed.* **2018**, *57*, 1888–1892. [CrossRef]
4. Férey, G.; Mellot-Draznieks, C.; Serre, C.; Millange, F.; Dutour, J.; Surblé, S.; Margiolaki, I. A Chromium Terephthalate-Based Solid with Unusually Large Pore Volumes and Surface Area. *Science* **2005**, *309*, 2040–2042. [CrossRef]
5. Xu, Z.-X.; Ma, Y.-L.; Zhang, L.-S.; Zhang, J. A couple of Co(II) enantiomers constructed from semirigid lactic acid derivatives. *Inorg. Chem. Commum.* **2016**, *73*, 115–118. [CrossRef]
6. Miao, S.; Sun, X.; Wang, K.; Xu, C.; Li, Z.; Wang, Z. Effect of Charge on the Structures of Zn(II) Coordination Polymers with Triazole-carboxylate Ligands: Syntheses, Structures, and Luminescent Properties. *Crystals* **2018**, *8*, 312. [CrossRef]
7. Xu, Z.-X.; Ma, Y.-L.; Lv, G.-L. Homochiral coordination polymers with helixes and metal clusters based on lactate derivatives. *J. Solid State Chem.* **2017**, *249*, 210–214. [CrossRef]
8. Gu, J.; Cai, Y.; Wen, M.; Ge, Z.; Kirillov, A.M. New Topologically Unique Metal-Organic Architectures Driven by a Pyridine-Tricarboxylate Building Block. *Crystals* **2018**, *8*, 353. [CrossRef]
9. Yang, Q.H.; Xu, Q.; Jiang, H.-L. Metal–organic frameworks meet metal nanoparticles: Synergistic effect for enhanced catalysis. *Chem. Soc. Rev.* **2017**, *46*, 4774–4808. [CrossRef]
10. An, W.; Aulakh, D.; Zhang, X.; Verdegaal, W.; Dunbar, K.R.; Wriedt, M. Switching of Adsorption Properties in a Zwitterionic Metal-Organic Framework Triggered by Photogenerated Radical Triplets. *Chem. Mater.* **2016**, *28*, 7825–7832. [CrossRef]
11. Huang, Y.-Q.; Cheng, H.-D.; Chen, H.-Y.; Wan, Y.; Liu, C.-L.; Zhao, Y.; Xiao, X.-F.; Chen, L.-H. Structural diversity in coordination polymers with a semirigid Lewis acidity ligand: Structures and properties. *CrystEngComm* **2015**, *17*, 5690–5701. [CrossRef]
12. Leroux, M.; Mercier, N.; Allain, M.; Dul, M.-C.; Dittmer, J.; Kassiba, A.H.; Bellat, J.-P.; Weber, G.; Bezverkhyy, I. Porous Coordination Polymer Based on Bipyridinium Carboxylate Linkers with High and Reversible Ammonia Uptake. *Inorg. Chem.* **2016**, *55*, 8587–8594. [CrossRef]
13. Wang, K.; Ma, Y.; Tang, H. Lanthanide Coordination Polymers as Luminescent Sensors for the Selective and Recyclable Detection of Acetone. *Crystals* **2017**, *7*, 199. [CrossRef]
14. Wang, K.-M.; Du, L.; Ma, Y.-L.; Zhao, J.-S.; Wang, Q.; Yan, T.; Zhao, Q.-H. Multifunctional chemical sensors and luminescent thermometers based on lanthanide metal–organic framework materials. *CrystEngComm* **2016**, *18*, 2690–2700. [CrossRef]
15. Pan, M.; Du, B.-B.; Zhu, Y.-X.; Yue, M.-Q.; Wei, Z.-W.; Su, C.-Y. Highly Efficient Visible-to-NIR Luminescence of Lanthanide(III) Complexes with Zwitterionic Ligands Bearing Charge-Transfer Character: Beyond Triplet Sensitization. *Chem. Eur. J.* **2016**, *22*, 2440–2451. [CrossRef]
16. Qin, L.; Lin, L.-X.; Fang, Z.-P.; Yang, S.-P.; Qiu, G.-H.; Chen, J.-X.; Chen, W.-H. A water-stable metal–organic framework of a zwitterionic carboxylate with dysprosium: A sensing platform for Ebolavirus RNA sequences. *Chem. Commun.* **2016**, *52*, 132–135. [CrossRef]
17. Gong, T.; Yang, X.; Fang, J.-J.; Sui, Q.; Xi, F.-G.; Gao, E.-Q. Distinct Chromic and Magnetic Properties of Metal-Organic Frameworks with a Redox Ligand. *ACS Appl. Mater. Interfaces* **2017**, *9*, 5503–5512. [CrossRef]
18. Higuchi, M.; Nakamura, K.; Horike, S.; Hijikata, Y.; Yanai, N.; Fukushima, T.; Kim, J.; Kato, K.; Takata, M.; Watanabe, D.; et al. Design of Flexible Lewis Acidic Sites in Porous Coordination Polymers by using the Viologen Moiety. *Angew. Chem. Int. Ed.* **2012**, *51*, 8369–8372. [CrossRef]

19. Wang, Y.; Yue, Q.; Gao, E.-Q. Effects of Metal Blending in Random Bimetallic Single-Chain Magnets: Synergetic, Antagonistic, or Innocent. *Chem. Eur. J.* **2017**, *23*, 896–904. [CrossRef]
20. Gong, T.; Lou, X.; Fang, J. A novel coordination polymer based on Co(II) hexanuclear clusters with azide and carboxylate bridges: Structure, magnetism and its application as a Li-ion battery anode. *Dalton Trans.* **2016**, *45*, 19109–19116. [CrossRef]
21. Bhalla, V.; Gupta, A.; Kumar, M.; Rao, D.S.S.; Prasad, S.K. Self-Assembled Pentacenequinone Derivative for Trace Detection of Picric Acid. *ACS Appl. Mater. Interfaces* **2013**, *5*, 672–679. [CrossRef]
22. Fu, H.-R.; Yan, L.-B.; Wu, N.-T.; Ma, L.-F.; Zang, S.-Q. Dual-emission MOF$\supset\bigcap$dye sensor for ratiometric fluorescence recognition of RDX and detection of a broad class of nitro-compounds. *J. Mater. Chem. A* **2018**, *6*, 9183–9191. [CrossRef]
23. Fu, H.-R.; Zhao, Y.; Xie, T.; Han, M.-L.; Ma, L.-F.; Zang, S.-Q. Stable dye-encapsulated indium–organic framework as dual-emitting sensor for the detection of $Hg^{2+}/Cr_2O_7^{2-}$ and a wide range of nitro-compounds. *J. Mater. Chem. C* **2018**, *6*, 6440–6448. [CrossRef]
24. Jin, J.-C.; Wu, J.; Liu, W.-C.; Ma, A.-Q.; Liu, J.-Q.; Singh, A.; Kumar, A. A new Zn(II) metal–organic framework having 3D $CdSO_4$ topology as luminescent sensor and photocatalyst for degradation of organic dyes. *New J. Chem.* **2018**, *42*, 2767–2775. [CrossRef]
25. Zhang, Y.-Q.; Blatov, V.A.; Zheng, T.-R.; Yang, C.-H.; Qian, L.-L.; Li, K.; Li, B.-L.; Wu, B. A luminescent zinc(II) coordination polymer with unusual (3,4,4)-coordinated self-catenated 3D network for selective detection of nitroaromatics and ferric and chromate ions: A versatile luminescent sensor. *Dalton Trans.* **2018**, *47*, 6189–6198. [CrossRef]
26. Zhang, L.; Kang, Z.; Xin, X.; Sun, D. Metal–organic frameworks based luminescent materials for nitroaromatics sensing. *CrystEngComm* **2016**, *18*, 193–206. [CrossRef]
27. Cui, Y.-J.; Zhang, J.; He, H.; Qian, G.-D. Photonic functional metal–organic frameworks. *Chem. Soc. Rev.* **2018**, *47*, 5740–5785. [CrossRef]
28. Zeng, X.-S.; Xu, H.-L.; Xu, Y.-C.; Li, X.-Q.; Nie, Z.-Y.; Gao, S.-Z.; Xiao, D.-R. A series of porous interpenetrating metal–organic frameworks based on fluorescent ligands for nitroaromatic explosive detection. *Inorg. Chem. Front.* **2018**, *5*, 1622–1632. [CrossRef]
29. Gupta, A.K.; Tomar, K.; Bharadwaj, P.K. Structural diversity of Zn(II) based coordination polymers constructed from a flexible carboxylate linker and pyridyl co-linkers: Fluorescence sensing of nitroaromatics. *New J. Chem.* **2017**, *41*, 14505–14515. [CrossRef]
30. Lustig, W.P.; Mukherjee, S.; Rudd, N.D.; Desai, A.V.; Li, J.; Ghosh, S.K. Metal–organic frameworks: Functional luminescent and photonic materials for sensing applications. *Chem. Soc. Rev.* **2017**, *46*, 3242–3285. [CrossRef]
31. Das, P.; Mandal, S.K. A dual-functionalized, luminescent and highly crystalline covalent organic framework: Molecular decoding strategies for VOCs and ultrafast TNP sensing. *J. Mater. Chem. A* **2018**, *6*, 16246–16256. [CrossRef]
32. Liu, X.Y.; Liu, B.; Li, G.H.; Liu, Y.L. Two anthracene-based metal–organic frameworks for highly effective photodegradation and luminescent detection in water. *J. Mater. Chem. A* **2018**, *6*, 17177–17185. [CrossRef]
33. Song, B.-Q.; Qin, C.; Zhang, Y.-T.; Wu, X.-S.; Yang, L.; Shao, K.-Z.; Su, Z.-M. Spontaneous chiral resolution of a rare 3D self-penetration coordination polymer for sensitive aqueous-phase detection of picric acid. *Dalton Trans.* **2015**, *44*, 18386–18394. [CrossRef]
34. Sheldrick, G.M. *SHELXS-97, Program for the Solution of Crystal Structures*; University of Göttingen: Göttingen, Germany, 1997.
35. Sheldrick, G.M. SHELXT-Integrated space-group and crystal-structure determination. *Acta Crystallogr.* **2015**, *71*, 3–8. [CrossRef]
36. Kent, C.A.; Liu, D.; Meyer, T.J.; Lin, W. Amplified Luminescence Quenching of Phosphorescent Metal–Organic Frameworks. *J. Am. Chem. Soc.* **2012**, *134*, 3991–3994. [CrossRef]
37. Liu, G.-Z.; Li, S.-H.; Li, X.-L.; Xin, L.-Y.; Wang, L.-Y. Three series of MOFs featuring various metal(II)-carboxylate chains cross-linked by dipyridyl-typed coligands: Synthesis, structure, and solvent-dependent luminescence. *CrystEngComm* **2013**, *15*, 4571–4580. [CrossRef]
38. Wu, Y.; Yang, G.-P.; Zhao, Y.; Wu, W.-P.; Liu, B.; Wang, Y.-Y. Three new solvent-directed Cd(II)-based MOFs with unique luminescent properties and highly selective sensors for $Cu^{2+}$ cations and nitrobenzene. *Dalton Trans.* **2015**, *44*, 3271–3277. [CrossRef]

39. Zhang, C.; Yan, Y.; Pan, Q.; Sun, L.; He, H.; Liu, Y.; Liang, Z.; Li, J. A microporous lanthanum metal–organic framework as a bi-functional chemosensor for the detection of picric acid and $Fe^{3+}$ ions. *Dalton Trans.* **2015**, *44*, 13340–13346. [CrossRef]
40. He, G.; Peng, H.; Liu, T.; Yang, M.; Zhang, Y.; Fang, Y. A novel picric acid film sensor via combination of the surface enrichment effect of chitosan films and the aggregation-induced emission effect of siloles. *J. Mater. Chem.* **2009**, *19*, 7347–7353. [CrossRef]
41. Zhou, X.-H.; Li, L.; Li, H.-H.; Li, A.; Yang, T.; Huang, W. A flexible Eu(III)-based metal–organic framework: Turn-off luminescent sensor for the detection of Fe(III) and picric acid. *Dalton Trans.* **2013**, *42*, 12403–12409. [CrossRef]
42. Hu, Y.; Ding, M.; Liu, X.; Sun, L.; Jiang, H. Rational synthesis of an exceptionally stable Zn(II) metal–organic framework for the highly selective and sensitive detection of picric acid. *Chem. Commun.* **2016**, *52*, 5734–5737. [CrossRef]
43. Ma, Y.-L.; Du, L.; Zhao, Q.-H. Synthesis, crystal structure, luminescent and magnetic properties of lanthanide coordination polymers based on a zwitterionic polycarboxylate ligand. *Inorg. Chem. Commum.* **2017**, *77*, 1–5. [CrossRef]
44. He, H.; Zhu, Q.-Q.; Sun, F.; Zhu, G. Two 3D Metal–Organic Frameworks Based on $Co^{II}$ and $Zn^{II}$ Clusters for Knoevenagel Condensation Reaction and Highly Selective Luminescence Sensing. *Cryst. Growth Des.* **2018**, *18*, 5573–5581. [CrossRef]
45. Wu, Z.F.; Gong, L.K.; Huang, X.Y. A Mg-CP with in situ encapsulated photochromic guest as sensitive fluorescence sensor for $Fe^{3+}/Cr^{3+}$ ions and nitro-explosives. *Inorg. Chem.* **2017**, *56*, 7397–7403. [CrossRef]
46. Xing, S.; Bing, Q.; Qi, H.; Liu, J.; Bai, T.; Li, G.; Shi, Z.; Feng, S.; Xu, R. Rational design and functionalization of a Zinc metal-organic framework for highly selective detection of 2,4,6-Trinitrophenol. *ACS Appl. Mater. Interfaces* **2017**, *9*, 23828–23835. [CrossRef]